Chinese Science Bulletin

A comparative study of magnetic properties between whole cells and isolated magnetosomes of *Magnetospirillum magneticum* AMB-1

LI JinHua[1,2,3], PAN YongXin[1,3†], LIU QingSong[3,4], QIN HuaFeng[4], DENG ChengLong[4], CHE RenChao[5] & YANG XinAn[5]

[1] Key Laboratory of the Earth's Deep Interior, Institute of Geology and Geophysics, Chinese Academy of Sciences, Beijing 100029, China;
[2] Graduate University of Chinese Academy of Sciences, Beijing 100049, China;
[3] Franco-Chinese Biomineralization and Nano-structures Laboratory, Beijing 100029, China;
[4] State Key Laboratory of Lithospheric Evolution, Institute of Geology and Geophysics, Chinese Academy of Sciences, Beijing 100029, China;
[5] Beijing National Laboratory for Condensed Matter Physics, Institute of Physics, Chinese Academy of Sciences, Beijing 100080, China

The magnetic properties of magnetosome magnetite are of interdisciplinary interest because magnetosomes are potential carriers of natural remanent magnetization and paleoenvironment, as well as novel nano-biomaterials in biotechnological and biomedical applications. We carried out magnetic and electron transmission microscopy analyses of fresh *Magnetospirillum magneticum* AMB-1 whole cells and isolated magnetosomes. Results revealed that AMB-1 synthesized single-domain magnetite magnetosomes, which are arranged in the form of linear fragmental chain. The distinct differences of magnetic properties between these two samples can be faithfully interpreted in terms of spatial arrangement of magnetosomes and magnetostatic interaction. For the whole cells, the strong intra-chain interactions and weak inter-chain interactions generate behaviors of non-interacting uniaxial single-domain particles. Its δ-ratio is 3.0 and passes the Moskowitz test. In contrast, the isolated magnetosome sample has reduced values of coercivity and δ-ratio (1.5), due to increasing three-dimensional magnetostatic interactions and collapse of magnetosome chains. These observations provide useful insights into applications of the biogenic magnetite (magnetosomes) in magnetic nano-materials and magnetofossils in the paleomagnetic and environmental magnetism.

Magnetospirillum magneticum AMB-1, isolated magnetosomes, hysteresis loop, FORC, Verwey transition, Moskowitz test

Magnetotactic bacteria (MTB) are a heterogeneous group of prokaryotes with the capability of synthesizing magnetosomes, which are intracellular, membrane-enveloped crystals of magnetite or greigite. The magnetosomes, ranging from 30 nm to 120 nm, are usually arranged in the form of single or multiple straight chains within cell, assisting the bacterium in orienting and swimming along the geomagnetic field lines[1,2]. In the past decade, the potential bionanomaterial and biomedical applications of magnetosomes have been highlighted due to their unique characteristics, i.e., narrow size range, perfect crystal morphology and high chemical purity[3,4]. Therefore, magnetic properties of magnetosomes have been of great interest in fields of environmental magnetism, paleomagnetism and biomagnetism, as well

Received January 15, 2009; accepted April 1, 2009
doi: 10.1007/s11434-009-0333-x
†Corresponding author (email: yxpan@mail.iggcas.ac.cn)
Supported by the National Natural Science Foundation of China (Grant Nos. 4082-1091 and 40325011), Hundred Talents Program of the Chinese Academy of Sciences and Marie-Curie Fellowship (IIF) Return Phase of (Grant No. MIF1-CT-2005-007555)

Citation: Li J H, Pan Y X, Liu Q S, et al. A comparative study of magnetic properties between whole cells and isolated magnetosomes of *Magnetospirillum magneticum* AMB-1. Chinese Sci Bull, doi: 10.1007/s11434-009-0333-x

as nano-biomaterial and biomedical utilization[5–11].

Rock magnetic parameter can reflect the nature of the magnetic minerals, grain size, domain states, and magnetostatic interactions. Therefore, rock magnetism is used as an important tool to study the magnetic properties of MTB produced magnetic crystals, including cultivated strains[12–17] and wild types[18,19]. Previous studies revealed that the linear magnetosome chain produces strong intra-chain magnetostatic interaction and has pronounced shape anisotropy[17,19], which may result in high δ-ratio value (>2), where δ-ratio is δ_{FC}/δ_{ZFC}, reflecting the difference of remanence losses across the Verwey transition between the field-cooled (FC) and zero-field-cooled (ZFC) processes. The δ-ratio therefore has been used to determine the presence of magnetofossils[8,16,18,19], known as the Moskowitz test[16]. The δ-ratio is reduced as the magnetosome were extracted from MTB cells and collapsed into a highly interacting system, such as a clump[16,20]. Other magnetic properties, e.g. coercivity (B_c), coercivity of remanence (B_{cr}), and the M_{rs}/M_s (M_{rs}, saturation remanence; M_s, saturation magnetization) can be influenced by magnetostatic interactions[12,16,17,20]. In other words, magnetic measurements are useful in unraveling the spatial arrangement and magnetostatic interaction of magnetosomes. Besides, previous investigations found that, for inorganic stoichiometric magnetite, the Verwey transition temperature (T_v) is ~120−125 K; magnetosome magnetite produced by cultivated and uncultivated MTB have lower T_v (100−110 K)[16,18,19,21,22]. Pan et al.[19] interpreted the reduced T_v as an intrinsic property of bacterial magnetosome magnetite.

Pure culture of MTB provides sufficient quantities of whole cells and isolated magnetosomes for magnetic measurements. Recently, Li et al.[23] reported that *Magnetospirillum magneticum* AMB-1, when grown in batch culture under microaerobic conditions, initiates to mineralize magnetosomes simultaneously at multiple sites within the cell body and finally forms a linearly fragmental chain consisting of 3 to 5 sub-chains. Both the T_v and B_c of whole cell samples increased with the growth of magnetosomes. The present study systematically compared the magnetic properties of fresh whole cells and isolated magnetosomes of AMB-1 after 96 h culture. The magnetic measurements included room-temperature hysteresis loops and first-order reversal curve (FORC) diagrams, Verwey transition and Moskowitz test. Finally, effects of magnetostatic interactions of magnetosomes on bulk magnetic properties of samples were discussed.

1 Material and methods

Strain AMB-1 (*Magnetospirillum* sp. ATCC 700264[24]) was grown in an enriched magnetic spirillum growth medium (MSGM) as previously described[25], with the addition of 60 μmol/L Fe-quinate. Total 5 L batch culture of cells was carried out statically at 26℃ for 96 h. Cells were harvested by centrifugation at 10000 r/min for 10 min at 4℃. Half of the centrifuged cells was suspended into 10 mL distilled water and was sonicated for 5 min with pulses of 5 s alternated with pauses of 5 s within ice bath using an ultrasonic disrupter (VCX130, SONICS, U.S.A.). The magnetosomes were magnetically purified by using a neodymium-boron magnet and were then washed with distilled water. This extraction process was repeated for 5 times, after which the magnetosomes were magnetically pelleted. The fresh samples of residual cell pellet and isolated magnetosomes were loaded into gelatin capsules and were immediately magnetically measured. To avoid possible oxidation, the whole process of magnetosome extracting and sample loading was carried out inside an anaerobic glove box (oxygen concentration lower than 0.03%).

The analyses of number, grain size, spatial arrangement, crystal structure and selected area electron diffraction (SAED) of magnetosomes were performed with a JEM2010 transmission electron microscope (TEM) (JEOL, Japan) operating at 200 kV.

Room-temperature hysteresis loops and FORCs were measured using a MicroMag 2900 Alternating Gradient Magnetometer (Princeton Measurements Corporation, sensitivity is 1.0×10^{-11} Am^2). Hysteresis loops were measured between ±1.0 T with an averaging time of 200 ms. Subsequently the saturation isothermal remanent magnetization (SIRM) acquired at 1.0 T was demagnetized in a backfield to obtain B_{cr}. FORCs were measured by following the protocol described by Roberts et al.[26]. FORC diagrams were calculated using the FORCinel version 1.05 software with a smoothing factor (SF) of 3[27]. Generally, in a FORC diagram, the horizontal axis H_c corresponds to the coercivity distribution and the vertical axis H_b corresponds to the distribution of interaction fields[26,28,29].

Low-temperature magnetic experiments were performed using a quantum design magnetometer (MPMS XP-5, sensitivity is 5.0×10^{-10} Am^2). Zero-field-cooled

(ZFC) and field-cooled (FC) curves were acquired by cooling the samples from 300 K to 5 K in a zero field and in a 5 T field, respectively, followed by giving a saturation isothermal remanent magnetization in a field of 5 T at 5 K (hereafter termed $SIRM_{5T\text{-}5K}$), and then measuring the remanent magnetization in zero field at intervals of 2−5 K upon warming to 300 K. The T_v is defined as the temperature for the maximum of the first-order derivative of the FC curve (dM/dT). The δ-ratio (δ_{FC}/δ_{ZFC}) was calculated after Moskowitz et al.[16]. The δ is defined as $(M_{80K}-M_{150K})/M_{80K}$, where M_{80K} and M_{150K} are the remanences measured at 80 K and 150 K, respectively.

2 Results

2.1 Spatial arrangement of magnetosomes

Figure 1(a) shows typical TEM images of linear arrangement of magnetosome sub-chains within whole AMB-1 cell body. Statistic results showed that the AMB-1 cells produced 14 magnetosomes per cell in average with a mean grain size of 45.6±12.3 nm. Most cells (> 90%) formed linearly fragmental chains consisting of 3 to 5 sub-chains separated by large gaps. Each sub-chain commonly contains 3 to 6 closely-aligned magnetosomes. These results are consistent with our previous observations[23].

As shown in Figure 1(b), the isolated magnetosomes exhibit a significantly different spatial arrangement of particles from within the whole counterparts. An overall feature is that magnetosome sub-chains were completely destroyed and were collapsed into aggregation with various spatial arrangements. More specifically, part of magnetosomes collapsed completely tends to closely pack into a clump. While the residual magnetosome chains, with part of the chains closed to form loops, seem to loosely aggregate. Higher-magnified TEM observations revealed that the magnetosome membranes were still intact and enveloped the isolated magnetosomes.

The SAED pattern and high resolution TEM (HRT-

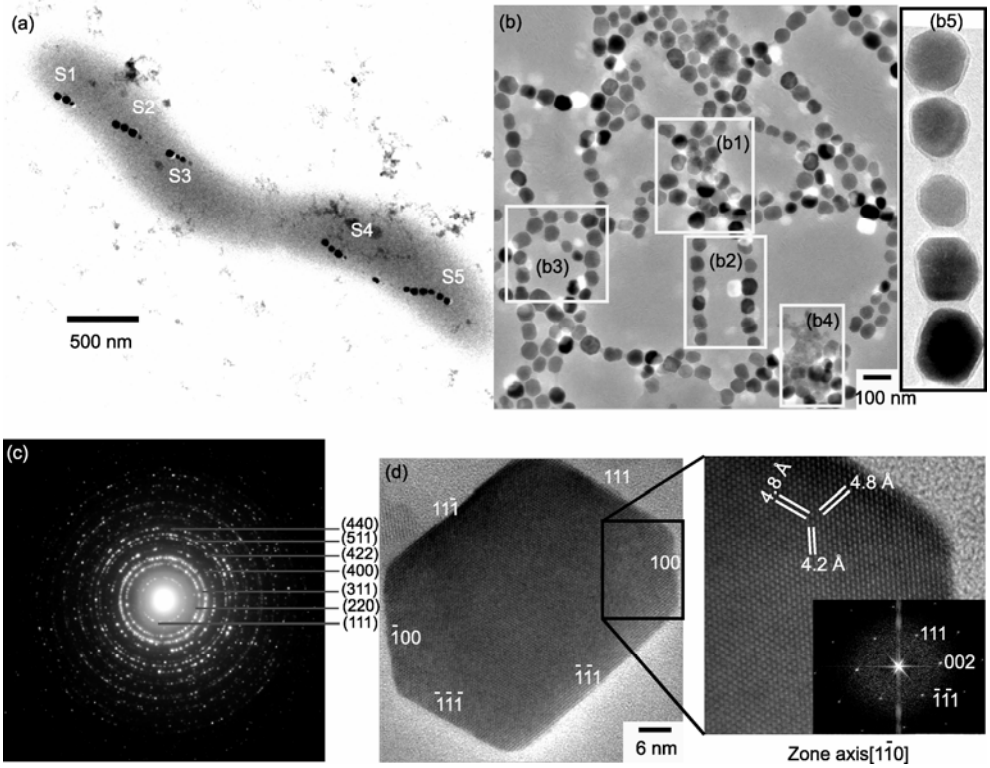

Figure 1 Representative TEM images of (a) whole AMB-1 cell showing magnetosome sub-chains, Sn (n = 1, 2,⋯) indicates sub-chain; (b) isolated magnetosomes, box-b1, -b2, -b3 and -b4 represent the magnetosome clump, residual magnetosome chains, magnetosome chain loops and magnetosomes bounded with residual cell debris, respectively, and box-b5 indicates the higher-magnified TEM image showing the intact magnetosome membranes; (c) SAED pattern of a group of isolated magnetosomes (camera length = 80 cm), the analyses of SAED pattern and characteristic d-spacings determined the single phase of magnetite for magnetosomes; (d) HRTEM images of a magnetosome crystal imaged in the [$11^{-}0$] zone, showing a well ordered single crystal structure with a cubo-octahedral crystal morphology, inset: magnification and Fourier transform of magnetosome marked by box. The spacings of 4.8 Å and 4.2 Å agree with those of the {111} and {002} lattice planes of magnetite, respectively.

EM) images indicate that magnetosomes produced by AMB-1 are well crystallized magnetite with cubo-octahedral crystal morphology (Figure 1(c), (d)).

2.2 Standard hysteresis parameters

Room-temperature hysteresis loops for the whole AMB-1 cells and their isolated magnetosomes are shown in Figure 2(a), (b), respectively. Both the hysteresis loops are closed at ~50 mT, saturated at low field (< 200 mT) and well characterized by the pot-bellied shape. However, the standard hysteresis parameters differ significantly. The whole cell sample shows typical Stoner-Wohlfarth type hysteresis loop and has the B_c, B_{cr}, B_{cr}/B_c and M_{rs}/M_s values of 18.6 mT, 23.3 mT, 1.25 and 0.46, respectively (Figure 2(a)). In comparison, the isolated magnetosome sample has the B_c, B_{cr}, B_{cr}/B_c and M_{rs}/M_s values of 12.2 mT, 18.2 mT, 1.5 and 0.33, respectively (Figure 2(b)).

2.3 FORC diagrams

As shown in Figure 3, the FORC distributions with well closed concentric contours around a central peak for both the samples indicate dominant single-domain (SD) behaviors of magnetosomes[26,28,29]. The peak coercivity, which is defined as the coercivity field corresponding to the peak of FORC distributions, is 29.8 mT and 21.2 mT for the whole cells and the isolated magnetosomes, respectively. Both of them are numerically larger than the B_{cr} values determined by their corresponding back-field demagnetization curves, possibly due to the asymmetry of coercivity distribution in the FORC diagrams.

The rather weak or negligible inter-sub-chain and inter-cell magnetostatic interactions are well exhibited by the rather narrow vertical spread along the H_c axis (<5 mT) in the FORC diagram (Figure 3(a). However, the FORC diagram for the isolated magnetosome sample shows a pronounced vertical spread with an order of nearly 20 mT at low coercivity regions (H_c = ~15 mT), indicating strong three-dimensional magnetostatic interactions. Additionally, this vertical distribution gradually constricted towards larger H_c and reached a similar level at H_c > 50 mT to that for the whole cell sample (Figure 3(b)). The FORC diagram with a slightly bimodal nature for the isolated magnetosomes is possibly due to the co-existence of the residual magnetosome chains (higher coercivity) and the close package of collapsed magnetosome chains (lower coercivity). The half-width field ($H_{b1/2}$), which is defined as the value of the interaction field where the peak of the FORC distribution has reduced to half of its maximum value, is 2.4 mT and 4.2 mT for the whole cells and isolated magnetosomes, respectively (Figure 3).

2.4 The Verwey transition and Moskowitz test

The thermal demagnetization curves for the whole cells and isolated magnetosomes are shown in Figure 4(a), (b), respectively. Both ZFC and FC curves show sharp drops in remanence intensity between 90 K and 110 K, which corresponds to the Verwey transition of magnetosome magnetite[16,18,19,21]. Both samples have consistent T_v of 106 K, lower than ~120−125 K for stoichiometric magnetite. The reduced T_v for AMB-1 magnetosomes, which is consistent with previous studies on cultivated or uncultivated MTB, is possibly due to the nonstoichiometry of magnetosome magnetite, i.e., ion vacancies or crystal defects. On the other hand, the distinct Verwey transition and same T_v values for both samples indicate that the T_v is not related to the spatial arrangements of magnetosomes. And the extracted magnetosomes did not undergo effects from oxidation, because any slight oxidization can shift the T_v to a lower temperature, as well as depress and broaden this transition[30].

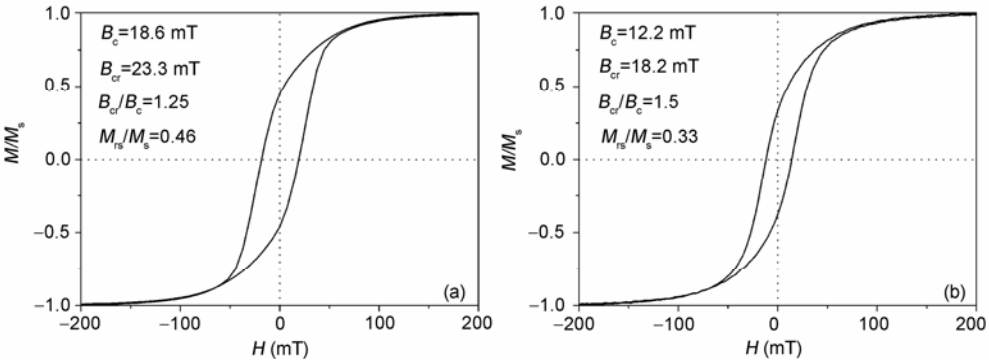

Figure 2 Normalized hysteresis loops for the whole AMB-1 cell sample (a) and the isolated magnetosome sample (b) at room temperature. B_c, B_{cr}, M_s and M_{rs} represent the coercivity, remanent coercivity, saturation magnetization and saturation remanence, respectively.

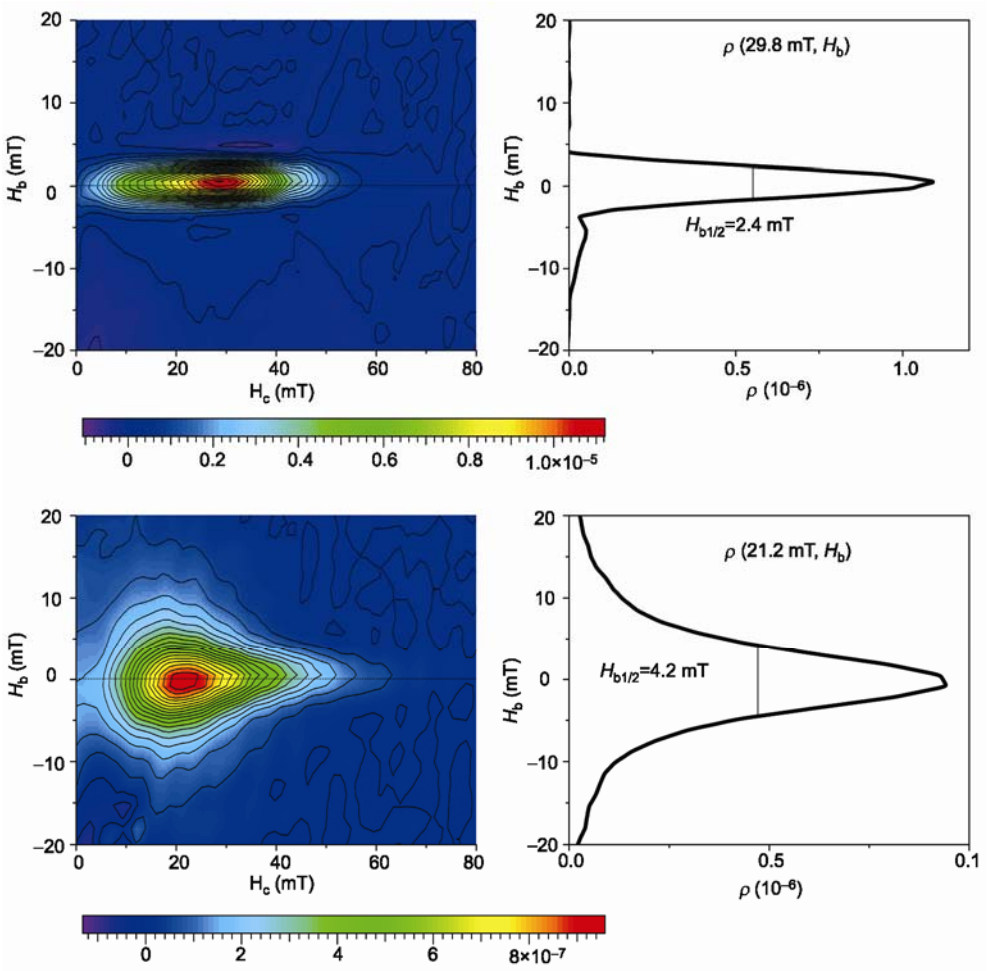

Figure 3 Room-temperature FORC diagrams for the whole AMB-1 cell sample (a) and the isolated magnetosome sample (b), both derived with a smooth factor of 3. Insets in (a) and (b): vertical profile through the peak of the FORC distribution rendering a measure of the half-width field ($H_{b1/2}$).

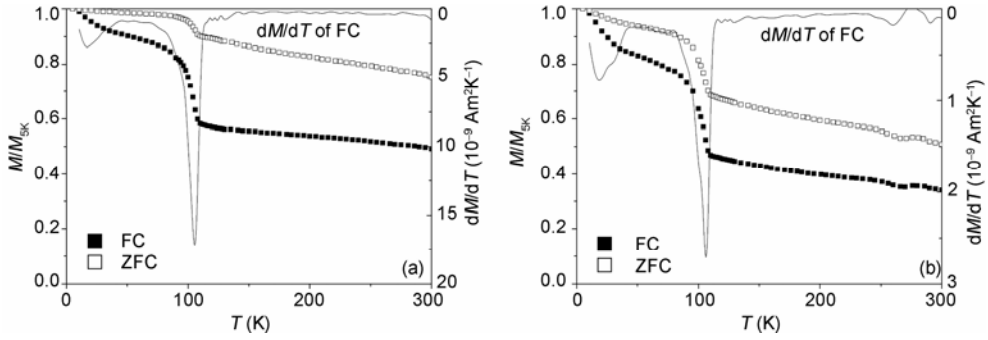

Figure 4 Normalized low-temperature saturation remanence demagnetization curves for the whole AMB-1 cell sample (a) and the isolated magnetosome sample (b) after the samples were pretreated in zero-field cooled (ZFC, open squares) and in field cooled (FC, solid squares).

Nevertheless, the remanence lost at T_v (δ_{FC} and δ_{ZFC}) is less for the whole cells than that for the isolated magnetosomes (Table 1). The δ_{FC}/δ_{ZFC} for the whole AMB-1 cell sample is 3.0, suggesting that the Moskowitz test is still valid for magnetosome sub-chains. Due to collapse of linearly fragmental chains into an interacting system, the isolated magnetosome sample has its δ_{FC}/δ_{ZFC} of 1.5, lower than the threshold of the Moskowitz test (2.0), but still larger than the δ-ratio values of inorganic magnetite samples[16]. Additionally, the isolated magnetosome sample exhibits a faster thermal decay on remanence below 30 K and above 120 K than the whole cell sample

(Table 1 and Figure 4). This suggests a higher degree of progressive unblocking of magnetization occurring in the isolated magnetosomes than in the whole cells, which indicates that there is a relatively higher contribution of superparamagnetic (SP) particles in the former than in the latter.

Table 1 Comparison of low-temperature magnetic parameters between the whole AMB-1 cell sample and the isolated magnetosome sample

Content	Whole cell sample	Isolated magnetosome sample
T_v [a)]	106 K	106 K
LTD_FC(5−30 K)% [b)]	7.0	12.9
LTD_FC(120−300 K)% [b)]	13.8	25.3
δ_{FC} [c)]	0.35	0.45
δ_{ZFC} [c)]	0.12	0.30
δ_{FC}/δ_{ZFC} [c)]	3.0	1.5

a), T_v, Verwey transition temperature, is determined by the maximum of the dM/dT of FC data; b) LTD_FC(X–Y K)% = (M_X–M_Y)/M_X×100; c) δ_{FC}, δ_{ZFC} and δ_{FC}/δ_{ZFC} were calculated after Moskowitz et al.[16].

3 Discussion

Previous studies revealed that the linearly magnetostatic interactions inside magnetosome chain lead to the entire chain to act as an elongated SD particle with high uniaxial shape anisotropy energy[31–34]. Some smaller magnetosomes located at ends of magnetosome chain could be constrained by intra-chain magnetostatic interactions[33]. Due to well separating of cytoplasm and high shape anisotropy energy of magnetosome chains, the sample consisting of randomly orienting whole MTB cells may behave as an isotropic ensemble of non-interacting uniaxial SD particles[17,19]. When grown microaerobically in batch culture, AMB-1 forms a linearly fragmental chain consisting of 3−5 sub-chains. The center-to-center distance between adjacent magnetosomes within sub-chains appears to be stable, and the distance between adjacent sub-chains is larger than 200 nm during the whole process of magnetosome formation[23].

The AMB-1 whole cell sample shows a typical Stoner-Wohlfarth type hysteresis loop and has a M_{rs}/M_s value very close to 0.5, which indicates the predominance of uniaxial SD behavior of sub-chains. For the isolated magnetosome sample, the disruption of cells and collapse of magnetosome sub-chains causes increasing contribution of SP behavior and significantly increasing negative magnetostatic interactions, i.e., inter-particle and inter-chain interactions. As a result, the low- and room-temperature magnetic properties significantly changed, e.g. B_{cr}, B_c, M_{rs}/M_s and δ_{FC}/δ_{ZFC} decrease, and B_{cr}/B_c, δ_{FC} and δ_{ZFC} increase. The $H_{b1/2}$ is 4.2 mT for the isolated magnetosome sample, higher than 2.4 mT for the whole cell sample, but much lower than 8.2 mT for the chemically synthesized SD magnetite powder (without biomembrane envelopment)[19]. This strongly indicates that the magnetosome membrane plays an essential role to decrease the magnetostatic interactiyns of magnetosome. The weak interactions can be helpful to dispersing magnetosomes uniformly within solution, which is crucial for the biomedical and biotechnological applications of isolated magnetosomes.

To identify magnetofossils from sediments or sedimentary rocks is important to reconstruct paleoenvironment. In natural environment, the magnetosome chains usually suffer more or less degree of chain collapse due to consolidation of sediments. The mixture of detrital magnetic minerals may make the detection of magnetofossils more complicated. Moskowitz et al.[16] proposed the threshold (1.5) of δ_{FC}/δ_{ZFC} for a positive chain response in mixtures of chains and inorganic magnetite. This value could be further reduced by higher content of detrital minerals and other effects. Pan et al.[8] measured two sediment samples with dead MTB from Lake Chiemsee, and obtained the δ_{FC}/δ_{ZFC} of 1.47 and 1.25 for the freeze-dried and air-dried samples, respectively. They interpreted the reduced δ_{FC}/δ_{ZFC} as a result of low-temperature oxidation and chain breakup. Our result corroborated these previous findings, suggesting that the δ_{FC}/δ_{ZFC} values ranging from 1.2 to 2.0 possibly imply that the presence of magnetosome chains suffered various degrees of either disruption or mixed with inorganic magnetic minerals or both. Therefore, rock magnetism with combination of multiple parameters is an important approach to rapidly identify magnetofossils in bulk sediment samples.

4 Conclusions

AMB-1 synthesizes magnetite magnetosomes in microaerobic batch culture. The whole AMB-1 cell sample shows significantly different magnetic properties from those of the isolated magnetosome sample. The former has a Stoner-Wohlfarth type hysteresis loop, narrow vertical spread in FORC diagram and high δ-ratio, while the latter has reduced B_c, B_{cr}, M_{rs}/M_s and δ-ratio due to collapse of magnetosome chains and increasing of magnetostatic interaction between magnetosome crystals.

Nevertheless, the magnetostatic interaction within the isolated magnetosomes is still lower than that of chemically synthesized magnetite (without biomembrane surrounding). Finally, our results suggest that the magnetostatic interactions possibly do not contribute to the lower T_V.

The authors thank Sun Lei and Wu Wenfang for their help in TEM observations and grain size measurement. They also thank two anonymous reviewers and the associate editor for their constructive suggestions to improve the manuscript.

1 Faivre D, Schüler D. Magnetotactic bacteria and magnetosomes. Chem Rev, 2008, 108: 4875－4898
2 Bazylinski D A, Frankel R B. Magnetosome formation in prokaryotes. Nat Rev Microbiol, 2004, 2: 217－230
3 Matsunaga T, Suzuki T, Tanaka M, et al. Molecular analysis of magnetotactic bacteria and development of functional bacterial magnetic particles for nano-biotechnology. Trends Biotechnol, 2007, 25: 182－188
4 Lang C, Schüler D, Faivre D. Synthesis of magnetite nanoparticles for bio- and nanotechnology: Genetic engineering and biomimetics of bacterial magnetosomes. Macromol Biosci, 2007, 7: 144－151
5 Kopp R E, Kirschvink J L. The identification and biogeochemical interpretation of fossil magnetotactic bacteria. Earth Sci Rev, 2008, 86: 42－61
6 Han L, Li S, Yang Y, et al. Comparison of magnetite nanocrystal formed by biomineralization and chemosynthesis. J Magn Magn Mater, 2007, 313: 236－242
7 Winklhofer M, Petersen N. Paleomagnetism and magnetic bacteria. In: Schüler D, ed. Magnereception and Magnetosomes in Bacteria. Berlin: Sringer-Verlag, 2006. 255－273
8 Pan Y X, Petersen N, Davila A F, et al. The detection of bacterial magnetite in recent sediments of Lake Chiemsee (southern Germany). Earth Planet Sci Lett, 2005, 232: 109－123
9 Pan Y X, Deng C L, Liu Q S, et al. Biomineralization and magnetism of bacterial magnetosomes. Chinese Sci Bull, 2004, 49: 2563－2568
10 Snowball I, Zillen L, Sandgren P. Bacterial magnetite in Swedish varved lake-sediments: a potential bio-marker of environmental change. Quat Int, 2002, 88: 13－19
11 Bazylinski D A, Moskowitz B M. Microbial biomineralization of magnetic iron minerals: microbiology, magnetism and environmental significance. Rev Mineral Geochem, 1997, 35: 181－223
12 Alphandery E, Ngo A T, Lefevre C, et al. Difference between the magnetic properties of the magnetotactic bacteria and those of the extracted magnetosomes: Influence of the distance between the chains of magnetosomes. J Phys Chem C, 2008, 112: 12304－12309
13 Pósfai M, Moskowitz B M, Arató B, et al. Properties of intracellular magnetite crystals produced by *Desulfovibrio magneticus* strain RS-1. Earth Planet Sci Lett, 2006, 249: 444－455
14 Kopp R E, Nash C Z, Kobayashi A, et al. Ferromagnetic resonance spectroscopy for assessment of magnetic anisotropy and magnetostatic interactions: A case study of mutant magnetotactic bacteria. J Geophys Res, 2006, 111: doi:10.1029/2006JB004529
15 Kobayashi A, Kirschvink J L, Nash C Z, et al. Experimental observation of magnetosome chain collapse in magnetotactic bacteria: Sedimentological, paleomagnetic, and evolutionary implications. Earth Planet Sci Lett, 2006, 245: 538－550
16 Moskowitz B M, Frankel R B, Bazylinski D A. Rock magnetic criteria for the detection of biogenic magnetite. Earth Planet Sci Lett, 1993, 120: 283－300
17 Moskowitz B M, Frankel R B, Flanders P J, et al. Magnetic properties of magnetotactic bacteria. J Magn Magn Mater, 1988, 73: 273－288
18 Moskowitz B M, Bazylinski D A, Egli R, et al. Magnetic properties of marine magnetotactic bacteria in a seasonally stratified coastal pond (Salt Pond, MA, USA). Geophys J Int, 2008, 174: 75－92
19 Pan Y X, Petersen N, Winklhofer M, et al. Rock magnetic properties of uncultured magnetotactic bacteria. Earth Planet Sci Lett, 2005, 237: 311－325
20 Kopp R E, Weiss B P, Maloof A C, et al. Chains, clumps, and strings: Magnetofossil taphonomy with ferromagnetic resonance spectroscopy. Earth Planet Sci Lett, 2006, 247: 10－25
21 Prozorov R, Prozorov T, Williams T J, et al. Magnetic irreversibility and Verwey transition in nano-crystalline bacterial magnetite. Phys Rev B, 2007, 76, doi:10.1103/physRevB1176.054406
22 Fischer H, Mastrogiacomo G, Löffler J F, et al. Ferromagnetic resonance and magnetic characteristics of intact magnetosome chains in *Magnetospirillum gryphiswaldense*. Earth Planet Sci Lett, 2008, 270: 200－208
23 Li J H, Pan Y X, Chen G J, et al. Magnetite magnetosome and fragmental chain formation of *Magnetospirillum magneticum* AMB-1: Transmission electron microscopy and magnetic observations. Geophys J Int, 2009, 177: 33－42
24 Matsunaga T, Sakaguchi T, Tadokoro F. Magnetite formation by a magnetic bacterium capable of growing aerobically. Appl Microbiol Biotechnol, 1991, 35: 651－655
25 Yang C D, Takeyama H, Tanaka T, et al. Effects of growth medium composition, iron sources and atmospheric oxygen concentrations on production of luciferase-bacterial magnetic particle complex by a recombinant *Magnetospirillum magneticum* AMB-1. Enzyme Microb Technol, 2001, 29: 13－19
26 Roberts A P, Pike C R, Verosub K L. First-order reversal curve diagrams: a new tool for characterizing the magnetic properties of natural samples. J Geophys Res, 2000, 105: 28461－28476
27 Harrison R J, Feinberg J M. FORCinel: an improved algorithm for calculating first-order reversal curve distributions using locally weighted regression smoothing. Geochem Geophys Geosyst, 2008, 9, doi:10.1029/2008GC001987
28 Pike C R, Roberts A P, Verosub K L. Characterizing interactions in fine magnetic particle systems using first order reversal curves. J Appl Phys, 1999, 85: 6660－6667
29 Qin H F, Liu Q S, Pan Y X. The first-order reversal curve (FORC) diagram: Theory and case study (in Chinese). Chin J Geophys, 2008, 51: 743－751
30 Özdemir Ö, Dunlop D J, Moskowitz B M. The effect of oxidation on the Verwey transition in magnetite. Geophys Res Lett, 1993, 20: 1671－1674
31 Pósfai M, Kasama T, Dunin-Borkowski R E. Characterization of bacterial magnetic nanostructures using high-resolution transmission electron microscopy and off-axis electron holography. In: Schüler D, ed. Magnetoreception and Magnetosomes in Bacteria. Berlin: Springer-Verlag, 2006. 197－225
32 Hanzlik M, Winklhofer M, Petersen N. Pulsed-field-remanence measurements on individual magnetotactic bacteria. J Magn Magn Mater, 2002, 248: 258－267
33 Dunin-Borkowski R E, McCartney M R, Frankel R B, et al. Magnetic microstructure of magnetotactic bacteria by electron holography. Science, 1998, 282: 1868－1870
34 Penninga I, Dewaard H, Moskowitz B M, et al. Remanence measurements on individual magnetotactic bacteria using a pulsed magnetic-field. J Magn Magn Mater, 1995, 149: 279－286